

Untethered magnetic millirobot for targeted drug delivery

Veronica Iacovacci¹ · Gioia Lucarini¹ · Leonardo Ricotti¹ · Paolo Dario¹ ·
Pierre E. Dupont² · Arianna Menciassi¹

Published online: 27 May 2015
© Springer Science+Business Media New York 2015

Abstract This paper reports the design and development of a novel millimeter-sized robotic system for targeted therapy. The proposed medical robot is conceived to perform therapy in relatively small diameter body canals (spine, urinary system, ovary, etc.), and to release several kinds of therapeutics, depending on the pathology to be treated. The robot is a nearly-buoyant bi-component system consisting of a carrier, in which the therapeutic agent is embedded, and a piston. The piston, by exploiting magnetic effects, docks with the carrier and compresses a drug-loaded hydrogel, thus activating the release mechanism. External magnetic fields are exploited to propel the robot towards the target region, while intermagnetic forces are exploited to trigger drug release. After designing and fabricating the robot, the system has been tested *in vitro* with an anticancer drug (doxorubicin) embedded in the carrier. The efficiency of the drug release mechanism has been demonstrated by both quantifying the amount of drug released and by assessing the efficacy of this therapeutic procedure on human bladder cancer cells.

Keywords Drug delivery system · Drug-loaded hydrogel · Magnetic robot · Magnetic docking · Microrobotics · Targeted therapy

Electronic supplementary material The online version of this article (doi:10.1007/s10544-015-9962-9) contains supplementary material, which is available to authorized users.

✉ Veronica Iacovacci
v.iacovacci@sssup.it

¹ The BioRobotics Institute, Scuola Superiore Sant'Anna, Viale Rinaldo Piaggio, 34, 56025 Pontedera, Pisa, Italy

² Department of Cardiac Surgery, Boston Children's Hospital, Harvard Medical School, Boston, MA 02115, USA

1 Introduction

The progressive development of new drug delivery systems is driven by the need to maximize therapy efficacy while minimizing negative side effects, typical of a systemic administration. To reach this goal, targeted drug delivery (TDD) systems can be employed; they allow, indeed, both a drug concentration increase in the region of interest and a marked reduction of side effects in the rest of the body (Ricotti et al. 2015).

Despite considerable advances in TDD technologies, most systems provide little control over timing or rate of release of the therapeutic agent and consequently cannot be tuned to patient needs and/or changes in physiological conditions. Triggerable drug delivery systems, on the contrary, can enable on-demand release by exploiting either the interaction between a “smart” material and the surrounding environment or by using a remotely controllable activation mechanism (Timko et al. 2010; Cassano and Trombino 2015).

A high-efficacy TDD system should enable the delivery of a therapeutic agent close to the target tissue in a highly controlled way. It should also assure drug release only when required. Currently available systems at the micro/nano-scale, such as magnetic nanoparticles (Arruebo et al. 2007) and smart triggerable materials (Hoare et al. 2011; Arruebo 2012; Chenga et al. 2013), often suffer from low controllability and from the impossibility of removing the delivery system after the therapy has been performed, thus raising toxicity-associated risks.

Medical robots have the potential to efficiently overcome some of these limitations, allowing targeted therapy at different length scales and in several body regions, by exploiting a wide network of small-diameter canals and endoluminal access points (Bergeles and Yang 2013). Robots' features, dimensions and operation mechanisms strongly depend on the procedure to be performed and, above all, on the working

environment (Li et al. 2004; Tabatabaei et al. 2012; Woods and Constandinou 2012; de Lanauze et al. 2013; Fusco et al. 2014). If we consider millimeter-sized body lumens, such as the central nervous system (CNS), in particular the spine, the urinary system, the pancreas or the ovary, therapy is usually performed through systemic drug administration in the case of chemotherapeutics for tumor treatment, catheters (e.g. those for chronic pain management in the spine), and other dedicated therapeutic/interventional instruments (such as hysteroscopes, special catheters, etc.) (Tobias et al. 1991; Storz 2015).

To overcome the low controllability of current TDD systems and the low dexterity and high stiffness of catheters (Chee and LeMoure 1995), an untethered robot able to controllably move through body channels and to perform on-demand drug administration would represent a valid solution. Due to space constraints (*i.e.* less than a few mm in most districts mentioned above), robot locomotion cannot be achieved by exploiting on-board actuators and power sources. It is therefore necessary to identify a propulsion strategy using energy provided by the environment or by an external source.

While several strategies have been proposed so far (Nelson et al. 2010), magnetic-based locomotion emerged as one of the most promising approaches. Thanks to their biocompatibility and efficiency also at the microscale (Abbott et al. 2009), magnetic fields can be exploited to wirelessly transmit high forces or torques with multiple degrees of freedom to miniature medical robots, thus allowing their locomotion through the human body (Abbott et al. 2007). Dedicated external platforms, based on permanent magnets (Fountain et al. 2010), electromagnets (Kummer et al. 2010) or magnetic resonance imaging (MRI) scanners (Kósa et al. 2011), have been recently exploited to produce pulling of magnetic microbeads, screw-like motion of helical artificial bacteria flagella (Mhanna et al. 2014) or swimming of magnetic microscallop (Qiu et al. 2014).

Microrobots' small size and payload-dependent swimming dynamics, however, make it challenging to translate these technologies in targeted therapy applications. At the same time, robotic systems for TDD, such as endoscopic capsules (Yim and Sitti 2012; Sliker and Ciuti 2014), possess limitations since they are too large to navigate through small body lumens, thus to get in hard-to-reach areas of the human body.

The contribution of this paper consists of the design and feasibility testing of a magnetically actuated two-component robot that is able to navigate through body canals such as the spine, the Wirsung duct and the urethra, for on-demand and *in situ* release of therapeutic agents (drugs, regenerative factors, etc.).

In particular, the design exploits the superposition of two different magnetic effects. An external magnetic field is used

to propel the two robot components to the neighborhood of the target site. Prior work has demonstrated that the same external magnetic field can be used to achieve independent control of multiple magnetic robots (Diller et al. 2012; Panagiotis et al. 2012; Eqtami et al. 2014). When drug release is desired, the external field can be used to bring the robots into close proximity, where intermagnetic attraction forces bring about docking and drug release.

The remainder of the paper is arranged as follows. The next section describes the design requirements of the robot and gives details on its design and fabrication, including synthesis and characterization of the drug-loaded hydrogel used for payload delivery. Finally, experimental evaluation is described, including an *in vitro* assessment of drug release profiles and response of human cancer cells to the treatment.

2 Materials and methods

2.1 System design: general considerations and working environment

The system consists of two millimeter-sized near-neutrally buoyant components (*i.e.* carrier and piston) both containing a spherical permanent magnet (Fig. 1). The carrier consists of a polymeric shell containing a drug-loaded hydrogel. Holes in the shell allow drug release. NdFeB powder embedded in its tip adds to total magnetization to increase heterogeneity and thus enhancing an independent control of the two robot components (Panagiotis et al. 2012; Eqtami et al. 2014). Once navigated to the target position shown in the Fig. 2, attraction between the magnetic materials of each component causes docking, during which the piston enters the mating cavity of the carrier, squeezes the hydrogel, and causes drug release.

Navigation of robot components can be performed using, *e.g.*, an MRI scanner, a coil system or permanent magnets. The devised therapeutic strategy is articulated in the following sequence of actions:

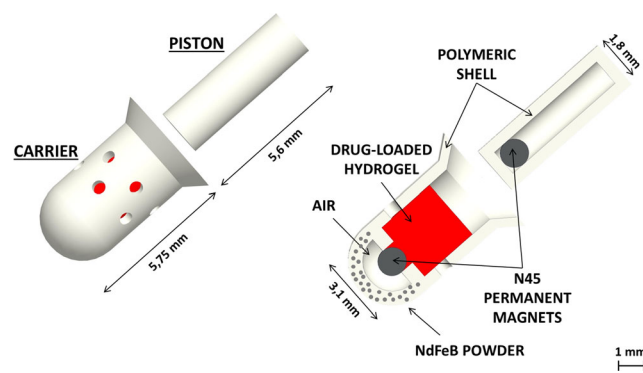
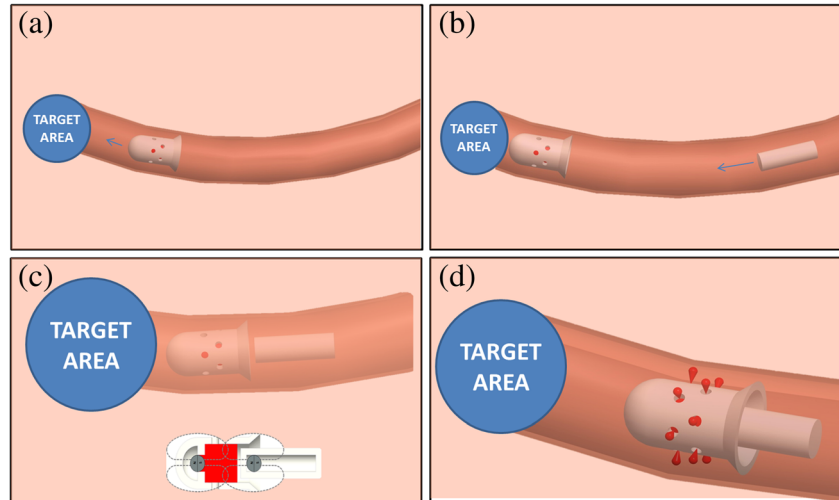


Fig. 1 Bi-component robot design and its constitutive elements

Fig. 2 Therapeutic procedure overview. **a** The carrier is injected and navigated to the target site. **b** The carrier is maintained approximately fixed and the piston is injected. **c** The piston is brought close to the carrier. Below a critical distance, attraction between the two modules prevails over the external magnetic control. **(d)** Docking occurs and the therapeutic agent is released



1. the carrier is injected into the desired body lumen and navigated to the target site (Fig. 2a), where it keeps the position;
2. the piston is subsequently injected and brought close to the target area as well (Fig. 2b). Thanks to the differences in terms of geometric and magnetic properties between the two robots, their locomotion can be controlled independently, as already demonstrated in the literature. Thus, the carrier can be kept approximately fixed, while the piston approaches;
3. the piston is brought close to the carrier. When the distance between the two components falls below a critical threshold, the magnetic attraction between the carrier and the piston prevails over the external control force (Fig. 2c) and docking between the parts occurs;
4. the piston compresses the drug-loaded hydrogel, thus triggering the release of the embedded therapeutic agent (Fig. 2d). The bi-component robot is then magnetically retrieved and extracted from the body.

The proposed robotic system is devised as a tool allowing clinicians to perform *in situ* release of drugs (chemotherapeutics, anti-inflammatory drugs, etc.) and regenerative factors in remote regions of the human body.

As mentioned, an untethered robotic system able to controllably move through a body channel can be a valid alternative to catheters (Tamaz et al. 2008) for targeted therapy procedures in body districts such as the CNS, the urinary system, the pancreas or the ovary. These sites can be reached, respectively, by crossing the subarachnoid space, the ureter (also allowing access to the prostate) and urethra, the excretory Wirsung duct, etc. These can be considered as relatively small diameter fluid-filled channels in which: (i) body fluids have features comparable with those of water in terms of viscosity and density; (ii) fluid flow rate can be approximated as zero and laminar behavior can be considered for robot motion;

(iii) robot diameter must be a few mm (Zaaron et al. 2006; Nelson et al. 2010) in order to enable locomotion through these body lumens.

2.2 Magnetic behavior

From the magnetic viewpoint, three different effects characterize the proposed robotic system: (i) magnetic locomotion, produced by an external magnetic platform, (ii) magnetic docking, produced by the interaction of on-board permanent magnets and enabling drug release triggering and (iii) differentiation of the two robots in terms of magnetic properties and drag profile. Each contribution is analyzed in more detail below.

- i) Locomotion. The locomotion and orientation of carrier and piston are obtained by generating suitable values of magnetic field and gradient. The magnetic forces and torques produced by an external source on the carrier and the piston can be expressed by:

$$\vec{F} = \vec{m} \cdot \nabla \vec{B} = V \vec{M} \cdot \nabla \vec{B} \quad (1)$$

$$\vec{T} = \vec{m} \times \vec{B} = V \vec{M} \times \vec{B} \quad (2)$$

where \mathbf{M} , \mathbf{B} , and $\nabla \mathbf{B}$ represent the magnetization of the carrier or the piston, the magnetic field and its gradient, respectively; V is the volume of the magnetic dipole.

- ii) Docking. The embedded permanent magnets serve both to enable robot locomotion and to activate the drug release mechanism. The idea is to exploit the attractive force between the on-board permanent magnets for robot docking and the consequent payload release. This force dominates external gradient forces when the robots approach each other (distance smaller than about 10 times the permanent magnet diameter). The interaction between piston and carrier can be modeled by

considering the magnets as magnetic dipoles characterized by a magnetic moment \mathbf{m} :

$$\vec{m}_i = V_i \vec{M}_i \quad (3)$$

The magnetic field \mathbf{B} produced by a magnetic dipole is (Yung et al. 1998):

$$\vec{B}(\vec{m}, \vec{r}) = \frac{\mu_0}{4\pi|r|^3} \left(3 \left(\vec{m} \cdot \frac{\vec{r}}{|r|} \right) \frac{\vec{r}}{|r|} - \vec{m} \right) + \frac{2\mu_0}{3} \vec{m} \delta^3(r) \quad (4)$$

where \mathbf{r} is the position vector connecting the dipole to the point of interest, μ_0 is the permeability of the free space and δ is the three-dimensional delta function. If

$$\vec{F}_m(m_1 \rightarrow m_2) = -\nabla \left(\vec{m}_2 \cdot -\vec{B}_1 \right) = \nabla \left(\vec{m}_2 \cdot \vec{B}_1 \right) = \frac{3\mu_0}{4\pi|r|^4} [(\hat{r} \times \vec{m}_1) \times \vec{m}_2 + (\hat{r} \times \vec{m}_2) \times \vec{m}_1 - 2\hat{r}(\vec{m}_1 \cdot \vec{m}_2) + 5\hat{r}((\hat{r} \times \vec{m}_1) \cdot (\hat{r} \times \vec{m}_2))] \quad (6)$$

The attraction force between the two permanent magnets corresponds to the compression force exerted by the piston on the drug-loaded hydrogel. This obviously influences the hydrogel choice, which must show properly tuned mechanical features.

iii) Independent navigation of robot components. NdFeB powders, located on the carrier head, contribute to differentiate the motion of the carrier and the piston in response to external magnetic fields (differences in geometrical cross section also contribute through variations in drag forces). Compared with traditionally employed superparamagnetic particles, NdFeB powders show a higher magnetic permeability, can be permanently magnetized and show a relatively low density in comparison with permanent magnets, thus not hampering robot buoyancy.

2.3 Gravity compensation

Gravity compensation is a key requirement for avoiding the contact between the robot and the working environment (thus minimizing friction and stiction issues) and achieving efficient three-dimensional navigation of miniaturized magnetic robots in fluids. Various gravity compensation techniques have been proposed for magnetic microrobots (Jeong et al. 2010; Mahoney et al. 2011; Sakar et al. 2013). In most of these cases, non-standard magnetic navigation systems able to generate magnetic gradients with tailored values are required in order to overcome friction forces.

In general, gravity compensation of magnetically propelled robots requires complex control methods together with a

the coordinate system is shifted to the center of the dipole and rotated such that the z-axis points in the same direction as \mathbf{m} , (4) can be simplified as follows:

$$\begin{aligned} B_z(\vec{r}) &= \frac{\mu_0}{4\pi} m \left(\frac{3\cos^2\theta-1}{|r|^3} \right) \\ B_x(\vec{r}) &= \frac{\mu_0}{4\pi} m \left(\frac{3\cos^2\theta-1}{|r|^3} \right) \end{aligned} \quad (5)$$

The angle θ is defined as $\theta=\varphi-\alpha$ where φ and α are the angles that \mathbf{m} and \mathbf{r} form with the z-axis, respectively. In our case, there are two dipoles that interact. The force exerted from one magnetic dipole (\mathbf{m}_1) on the other (\mathbf{m}_2) is:

substantially increased magnetic gradient demand. In order to reduce the impact of these constraints, the gravitational force should be minimized. This can be achieved only by minimizing the density differences between the robot and the surrounding environment. Palagi et al. (2013) proposed a solution based on nearly-neutrally buoyant hydrogel robots and demonstrated that, despite their relatively weak magnetic properties, for certain size/velocity ranges they could be more easily and efficiently propelled than state-of-the-art metal millirobots.

As an alternative to embedding a low-density material in the robot (such as dodecane which is highly toxic), a pre-determined volume of air may be introduced in the structure (Diller et al. 2013). This second approach has been pursued in this work. In order to be nearly-neutrally buoyant, the mean density of the robot should be the same of the fluid where it swims. By approximating the density of the human body fluids (that represent the workspace of the proposed robotic system) to that of water and by taking into account the specific density (ρ_i) and the correspondent volume (V_i) of the materials constituting the carrier and the piston, near-neutral buoyancy is guaranteed by the following equilibrium equation:

$$V_{tot} \times \rho_{water} = \sum_{i=0}^n V_i \times \rho_i \quad (7)$$

In the equation, n is the number of the materials, V_{tot} is the total volume of the robot and ρ_{water} is the water density. This equation was taken into account during the robot design phase in order to identify the volume of air needed both in the piston

and in the carrier as well as the appropriate volumetric proportion between the different materials, whose densities are reported in Table 1.

2.4 Drug-loaded hydrogel

In the design of this millirobotic system, a significant challenge is the selection of the drug-embedding material. Hydrogels are 3D networks composed of chemically or physically cross-linked hydrophilic polymer chains. They can be cast into almost any shape, size, or form and can absorb thousands of times their dry weight of water. It is possible to engineer hydrogels to resemble the extracellular environment in ways that enable their use in medical implants, biosensors, and devices for drug delivery (Seliktar 2012). A particular favorable class of hydrogels for drug delivery is based on agar and gelatin. They are biocompatible and can be infused not only with drugs, but also with cells that may release molecules promoting tissue regeneration (*e.g.* paracrine factors produced by stem cells) (Ricotti and Menciassi 2013; Alvarado-Velez et al. 2014; Gnavi et al. 2014; Tonda-Turo et al. 2014).

Different hydrogel compositions were mechanically tested to evaluate the Young's compression modulus. Gelatin percentage was fixed at 1 % *w/w* whereas agar concentration was varied (4, 2, 1, 0.75, 0.5 and 0.25 % *w/w*) in order to tune hydrogel mechanical properties. Agar (Sigma Aldrich, A9539) was dissolved in deionized water (d-H₂O) at 90 °C for about 15 min, under stirring. Then, the temperature was lowered to 50 °C and gelatin (Sigma Aldrich, G1890) was added and dissolved for 15 min, under stirring. To verify if the chosen hydrogel was actually able to embed therapeutics and if it was able to release them after squeezing, doxorubicin was included in the hydrogel matrix. Doxorubicin is a common anticancer drug that can be exploited for the treatment of many different kinds of tumor, ranging from breast, ovary and bladder cancer (Smith et al. 2006; Lammer et al. 2010; Tao et al. 2011). Doxorubicin hydrochloride (Sigma Aldrich, 44583) was added at a concentration of 200 µg/ml to the agar-gelatin solution, after lowering the temperature down to 40 °C. The solution was stirred for 2 min, before pouring the compound into petri dishes (to get samples for compression tests) or injecting it into the carrier (to assemble the drug-loaded robot). After pouring or injecting the solution, it solidified in a few minutes by physical cross-linking.

Table 1 Density of robot constitutive components

Material	Density [Kg m ⁻³]
NdFeB	7850
Hydrogel	1000
PDMS	952
Air	1.225

Assessing the hydrogel mechanical properties was crucial to identify which composition better suited the design requirements. Under the action of the compression force, corresponding to the attraction force between the two magnetic dipoles (expressed in Equation 6), the hydrogel is deformed and releases the infused drug. In compression, the drug-loaded matrix mechanical behavior should be such to allow an efficient squeezing process, despite the low squeezing force available, avoiding, at the same time hydrogel fracture (indeed, the leakage of hydrogel fragments could produce channel obstruction or undesired drug delivery into other regions). Moreover, the hydrogel should be able to stably embed drugs, thus releasing them only in presence of the triggering effect (*i.e.* mechanical compression).

Mechanical testing of the hydrogel compositions stated above were carried out in compression by using an Instron machine (Instron 4464), equipped with a ±10 N static load cell. A 0.5 mm/min compression speed was applied on cylindrical samples immersed in Phosphate Buffered Saline (PBS) solution. Using stress-strain curves obtained for each hydrogel composition, finite element model (FEM) simulations were carried out using Abaqus and MATLAB® to calculate the deformation produced on the hydrogel cylinder, due to the compression exerted by the piston.

The magnetic force was calculated analytically from Equation 6 and exploited in the model in order to simulate the effects produced on each agar-gelatin hydrogel type. The stress-strain curves were imported into Abaqus using the Hyperplastic module. In the Abaqus Step module, explicit dynamics was defined by imposing a mass scaling equal to 100. Appropriate tie constraints between the described elements were implemented, thus reproducing the microrobotic platform. The elements were meshed by using a structured Hex mesh. In particular, the simulations were used to define the composition that confers the highest deformation to the hydrogel without causing its fracture. Once the best composition was identified, further mechanical tests were carried out on the chosen hydrogel loaded with the drug, in order to verify whether the material properties were affected by doxorubicin embedding.

2.5 Polymeric shell and robot fabrication

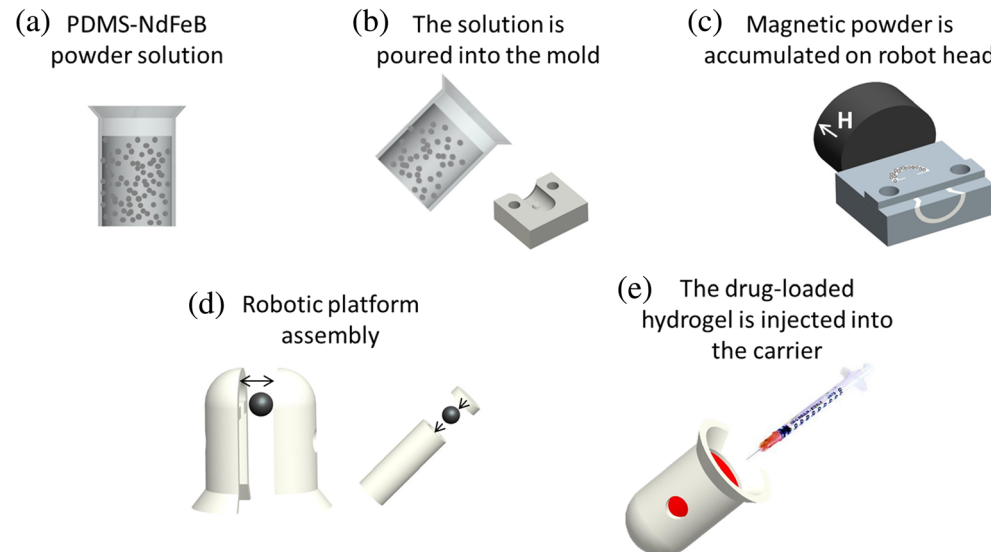
Using soft structures for the robot components is advantageous for reducing the risk of inducing damages to the biological channel. At the same time, some stiffness is required to avoid piston bending during docking and to ensure an efficient hydrogel compression. To balance these two needs, polydimethylsiloxane (PDMS, SYLGARD® 184, Dow Corning) was chosen. This material is biocompatible and its mechanical properties can be easily tuned by varying the monomer-curing agent ratio. Both the carrier and the piston were fabricated in

PDMS with a 5:1 monomer-curing agent ratio (Armani et al. 1999).

Robot dimensions are critical in terms of fabrication, as the robot is neither small enough (micrometer range) to justify the use of microfabrication techniques, nor sufficiently large to exploit traditional machining tools. Custom molds were fabricated through 3D-printing (3DSYSTEM PROJET HD 3000) and used to obtain the robot components. NdFeB powders (Magnequench Mqa-37-11, MolyCorp) were added at a concentration of 15 % w/w to the PDMS solution (Fig. 3a) and properly mixed. The obtained solution was then poured into the molds (Fig. 3b). Magnetic powders were accumulated at the top of the carrier's head to differentiate the carrier magnetization with respect to the piston (embedding only the permanent magnet), thus enabling their independent control. To collect the powders at the top of the carrier's head and to align powder particles, a dedicated setup was exploited (Fig. 3c). A permanent magnet was placed adjacent to the mold during the polymerization process (carried out at room temperature for 24 h). The proximity of a permanent magnet to the robot head produced a migration of the powders towards it, thus enhancing its accumulation and orientation. Before assembling the carrier components and permanent magnet (N45, diameter 1 mm) (Fig. 3d), the polymeric shell was permanently magnetized: a static magnetic field of at least 2T was required to magnetize the NdFeB powders. To this aim, a clinical 3T MRI scanner (Signa 3T GE scanner) was exploited, by aligning the robot axis with the direction of the scanner static magnetic field.

Once fabricated and assembled, 10 μ L of “hydrogel+drug” solution were injected into the carrier and let solidify *in situ* (Fig. 3e).

Fig. 3 Robot fabrication procedure. **a** NdFeB powders are added to the PDMS polymeric solution. **b** The compound is poured into the molds. **c** Permanent magnet causes powders to accumulate at the robot's head. After demolding, the carrier components with embedded powder are permanently magnetized by means of an MRI scanner. **d** The piston and the carrier are assembled, by also embedding a spherical permanent magnet. **e** The hydrogel is injected into the carrier



2.6 Locomotion and docking tests

Once fabricated the robot prototypes, operation tests were carried out to verify if the system was actually able to perform the desired task. First of all, a locomotion test was performed.

A customized PDMS arena (72 mm \times 36 mm \times 15 mm) with a channel (diameter and depth of 15 mm and 7.5 mm, respectively) and a circular chamber (diameter and depth of 30 mm and 10 mm, respectively) was fabricated by using a 5:1 monomer-curing agent ratio.

Both the carrier and the piston were accurately oriented and moved towards a desired position. A magnetic field of 5.2 mT and a magnetic field gradient of 0.05 T/m were generated by means of a permanent magnet placed below the workspace. This was exploited to bring the carrier and the piston to the target sites. In order to achieve the complete procedure illustrated in Fig. 2, the carrier was held at the desired position using an additional magnetic field of 50 mT, while the piston was navigated into position for docking.

2.7 Drug release tests

Drug release tests were performed to quantitatively assess the amount of drug released by the robot. These tests considered both the pre-docking state, to verify that premature drug leakage did not occur, and the docked configuration, to verify that a significant amount of drug was released.

To measure the amount of drug released by the robot, a spectrophotometric plate reader was used (PerkinElmer, VICTOR X3), by setting an excitation wavelength of 470 nm and an emission wavelength of 585 nm. A drug calibration curve was first obtained. Aqueous doxorubicin solutions at different drug concentrations were prepared and absorbance measures were carried out in triplicate for each concentration (200 μ L samples). Six different doxorubicin concentrations in the 0–

30 µg/mL range were tested, and experimental data were interpolated with an exponential function to draw the drug calibration curve.

Once obtained the calibration curve, *in vitro* release tests were performed. The amounts of doxorubicin released by the robots in the docked configuration were compared with control samples (in which no hydrogel squeezing occurred). In all these tests, robots were immersed in 1 mL of d-H₂O within a 48 multi-well plate. To measure drug release and its temporal profile, samples were taken at 30 s, 120 s, 210 s, 300 s, 600 s and 1200 s after either immersion of the robot in water or robot docking. At each time-point, 500 µL of solution were collected and gently replaced with 500 µL of d-H₂O, avoiding any external mechanical stimulation that may cause undesired drug release. Absorbance data were converted into drug quantity values and plotted as a function of time. Three independent samples were tested for each sample type. In addition, each absorbance reading was carried out in triplicate.

2.8 In vitro tests on cancer cells

In vitro efficacy tests were carried out on T24 human urinary bladder carcinoma cells (ATCC®, HTB-4™). The idea was to test the robotic system on unhealthy cells deriving from a district reachable with the proposed system, in order to prove the validity of the proposed approach.

Cells (passage number: < 3) were seeded in a standard multi-well plate at a density of 10,000 cells/cm² and kept in culture medium, composed of McCoy's 5a Medium Modified (ATCC®, 30-2007) supplemented with 10 % Fetal Bovine Serum (FBS, Euroclone), 100 IU/ml penicillin (EuroClone) and 100 mg/ml streptomycin (EuroClone). During culture, the cells were maintained at 37 °C in a saturated humidity atmosphere containing 95 % air and 5 % CO₂.

Four experimental groups were considered: (*i*) non treated cells ("negative control" samples); (*ii*) cells treated by immersing for 20 min a UV-sterilized carrier (undocked) in the culture medium ("undocked robot" samples); (*iii*) cells treated by immersing for 20 min a UV-sterilized carrier together with the piston in the culture medium ("docked robot" samples) and (*iv*) cells treated by directly dispersing doxorubicin in the culture medium at a concentration of 10 µg/mL ("positive control" samples).

Twenty-four hours after the testing of all these experimental groups, the samples were treated to assess reactive oxygen species (ROS) production. ROS generation is enhanced in cells, under conditions of oxidative stress, which lately cause alteration of membrane lipids, proteins, and nucleic acids. ROS production in T24 cells was detected by using a Reactive Oxygen Species Detection kit (Life Technologies, I36007). The assay is based on 5-(and-6)-carboxy-2',7'-

dichlorodihydrofluorescein diacetate (carboxy-H2DCFDA), which is a fluorogenic marker for ROS in viable cells. At the desired time-point the culture medium was removed, cells were rinsed with PBS and incubated for 45 min with a 25 µM carboxy-H2DCFDA working solution (in DMSO:PBS at 1:400 v/v), then immediately observed by means of a fluorescence microscope (Eclipse Ti, FITC-TRITC filters, Nikon) equipped with a CCD camera (DS-5MC USB2, Nikon and with NIS Elements imaging software).

Three days after the testing of the mentioned experimental groups, the extent of cell proliferation was quantified for the different sample types, by measuring deoxyribonucleic acid (DNA) content. In brief, at the desired time-point culture medium was removed, cells were rinsed with PBS and then treated with 500 µL of d-H₂O. Cell lysates were obtained by two freeze/thaw cycles of the samples (overnight freezing at -20 °C and 15 min thawing at 37 °C in an ultrasonication bath) to enable the DNA to go into the aqueous media. The DNA content in cell lysates was measured by using the PicoGreen kit (Life Technologies, P7519). Working buffer and PicoGreen dye solution were prepared and added according to the manufacturer's instructions (100 and 150 µL/well, respectively). After 10 min of incubation in the dark at room temperature, fluorescence intensity was measured on the microplate reader, using an excitation wavelength of 485 nm and an emission wavelength of 535 nm. For DNA quantification, three independent samples were analyzed for each sample type, and the volume analyzed for each sample was read in triplicate, in the microplate.

2.9 Statistical analyses

Analysis of variance was used to evaluate statistically significant differences among samples. A t-test was performed for comparison between two groups, while Holm–Sidak tests were performed for comparisons among several groups. Significance was set at 5 %.

3 Results and discussion

3.1 Hydrogel characterization and FEM simulations

Six hydrogel compositions, differing in agar concentration, were mechanically tested to identify which was the most suitable for the envisioned application (Online Resource 1). FEM simulations were carried out by using the stress-strain curves obtained through compression tests and the force values obtained by the dipole-dipole magnetic model (expressed in Equation 6). In particular, since at the squeezing starting point

the distance between the centers of the permanent magnets is 3.5 mm (the hydrogel cylinder is 2.5 mm high), a magnetic attraction force equal to 1.3 mN was considered. Figure 4 shows the simulation results and, in particular, how the deformation produced on the hydrogel changes with its agar content. Simulations demonstrated that a 0.25 % agar-1 % gelatin hydrogel, which represents the lower bound agar concentration to have a semi-solid behavior, undergoes a deformation of about 38 % while maintaining its integrity, thus leading to the choice of this composition for the drug-loaded matrix embedded in the carrier. Further compression tests and simulations were carried out on 0.25 % agar-1 % gelatin hydrogels incorporating doxorubicin. Simulations showed that the drug does not negatively affect hydrogel compression. On the contrary, hydrogel compression increases with doxorubicin inclusion, reaching a deformation of 43 % without compromising hydrogel integrity, thus further validating the choice of such drug delivery matrix.

3.2 Robot prototype, characterization and locomotion testing

After fabricating them, robot prototypes were inspected by means of a Hirox optical microscope (Fig. 5a–b) in order to evaluate their morphology and to remove residual materials. Figure 5c–f show that the robot was easily provided with the

doxorubicin-loaded hydrogel, which solidified in the robot and could be squeezed, when required.

Two types of carrier were produced, namely integrating or not NdFeB powders into the structure. The carriers with the embedded powders were permanently magnetized, as described in Materials and Methods section. Magnetic field measurements were performed by means of a Hall effect probe (Magnetometer KOSVAHA 5, Wuntronic). The objective was to demonstrate that the addition of NdFeB powders was actually able to contribute to robot magnetization. This is particularly important to differentiate the piston and the carrier in terms of magnetic properties despite the fact that they embed the same permanent magnet, thus to allow their independent motion control. Magnetic field measures were carried out by placing the Hall effect probe in contact with the carrier's head. Results demonstrated that the NdFeB powders contributed in differentiating the carrier from the piston: in absence of NdFeB powders, the measured field was 37 ± 4.2 G, while for the carriers embedding the powders it was 102.5 ± 22.6 G.

Then, a preliminary evaluation was performed in order to demonstrate the controllability of robot locomotion and of the docking procedure. The results are shown in the attached video (Online Resource 2) and in Fig. 6. They demonstrated that both the components can be moved in a liquid environment thanks to their buoyancy and to magnetic fields and that the procedure depicted in Fig. 2 is feasible with the achieved prototype.

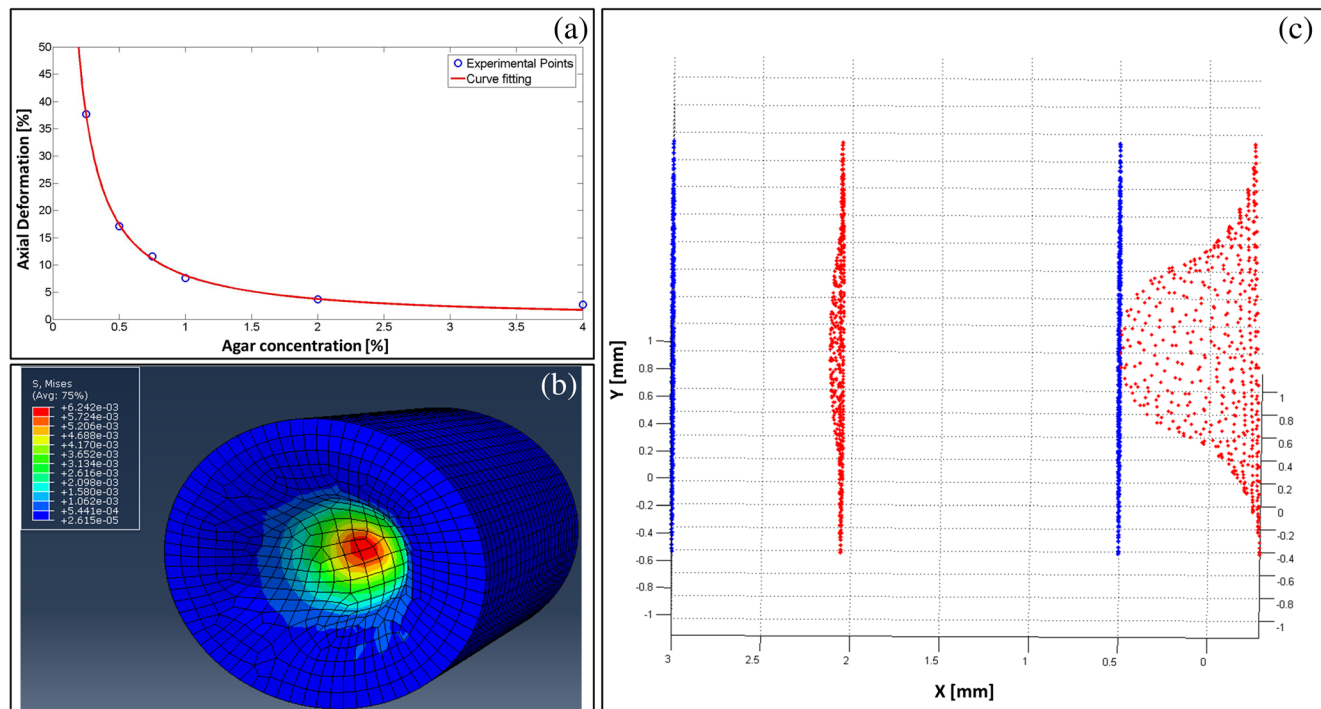
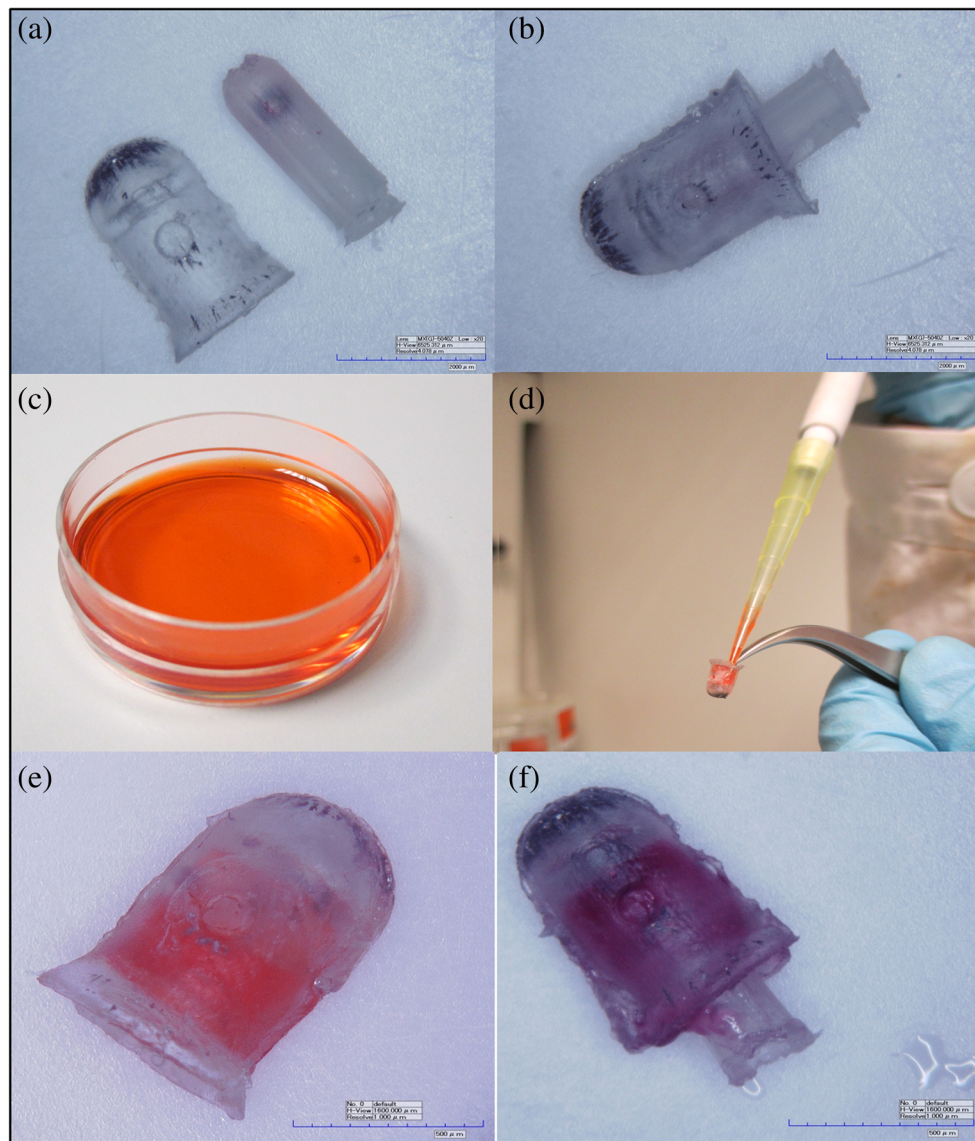


Fig. 4 Abaqus FEM simulation results. **a** Hydrogel deformation produced by magnetic attraction force as a function of agar concentration. **b** Distribution of stress on the chosen hydrogel. **c**

Deformation of the 0.25 % agar-1 % gelatin hydrogel after squeezing (blue and red lines refer to the initial and the final surface of the hydrogel, respectively)

Fig. 5 **a** Images of carrier and piston obtained through a Hirox microscope. **b** Robot prototype in the docked configuration. **c** Drug-loaded agar-gelatin hydrogel. **d** Procedure of drug-loaded hydrogel injection into the carrier. **e** Carrier prototype with drug-loaded hydrogel embedded. **f** Docked configuration, with the hydrogel squeezed



3.3 Drug release and *in vitro* validation

Release tests carried out on the fabricated prototypes confirmed the correct operation of the robotic system. The doxorubicin calibration curve (Fig. 7a) was achieved by interpolating experimental absorbance points with an exponential function and was used to evaluate the amount of drug released by the robots. Figure 7b shows the temporal release profile for both docked and undocked robots. The results demonstrate that squeezing is crucial for drug release activation, since in the absence of squeezing (control samples) the spontaneous release was nearly zero.

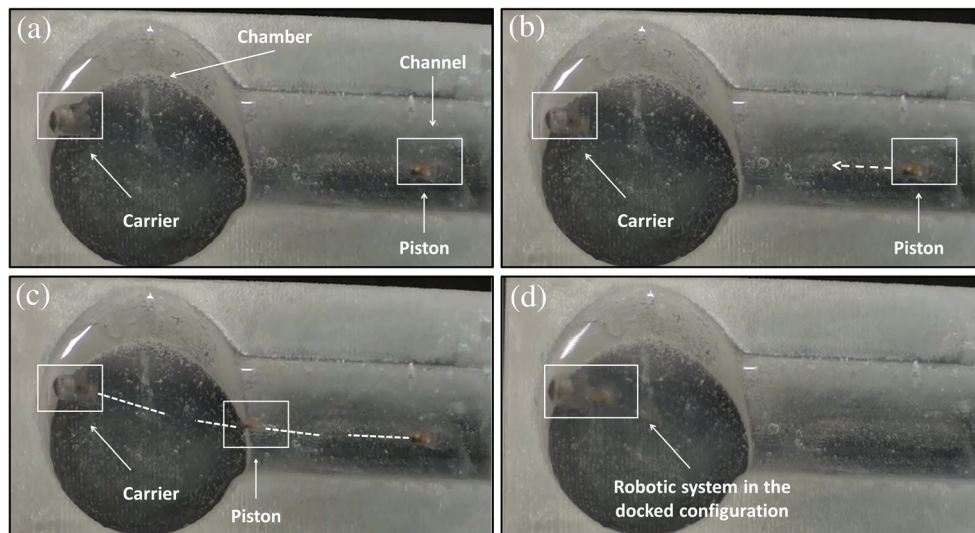
Furthermore, the release trend revealed that drug release was still ongoing after 20 min. This represents a reasonable duration for the therapeutic procedure. By integrating the discrete values measured through spectrophotometric analysis at each sampling time, the total amount of doxorubicin released

was calculated (Fig. 7c); these quantitative data confirmed that the docking between the carrier and the piston efficiently triggered drug release.

While the net amount of drug released by each robot is quite low (only a few ng), this amount is reasonable since the drug is highly effective at low concentrations and is released directly at the damaged site (Zhao et al. 2011). Furthermore, the amount of drug released prior to docking is only 0.7 % of that achieved through docking.

In vitro tests using T24 cells confirmed that the prototype was effective as an anticancer targeted therapeutic platform. Figure 8a shows the ROS production for the different sample types tested. While “negative control” and “undocked robot” samples showed no detectable trace of ROS, “docked robot” samples were characterized by a diffuse red fluorescence, similar (although less intense) to that of “positive control” samples. DNA measurements (Fig. 8b) confirm this trend:

Fig. 6 Experimental validation of navigation and docking. A magnetic field of 5.2 mT and a magnetic field gradient of 0.05 T/m were generated by means of a permanent magnet placed below the workspace. **a** The carrier is kept fixed in the target position and the piston is injected into the PDMS channel. **b** The piston is oriented for navigation to the target. **c** Piston path towards the carrier. **d** Docking of the carrier and the piston



“docked robot” samples, similarly to “positive control” samples, showed a marked reduction in cell proliferation, at day 3 after docking tests. “Undocked robot” samples showed a much higher DNA content, although smaller than “negative control” samples. This is probably because the small drug quantity released by the undocked robot during the considered

time did have an effect. In practice, this can be considered a negligible factor, since in a real clinical scenario, the undocked robot would not remain for 20 min in the same position: it will travel, in fact, through the targeted canal. Therefore, the undesired effect revealed by *in vitro* tests would be strongly mitigated, *in vivo*.

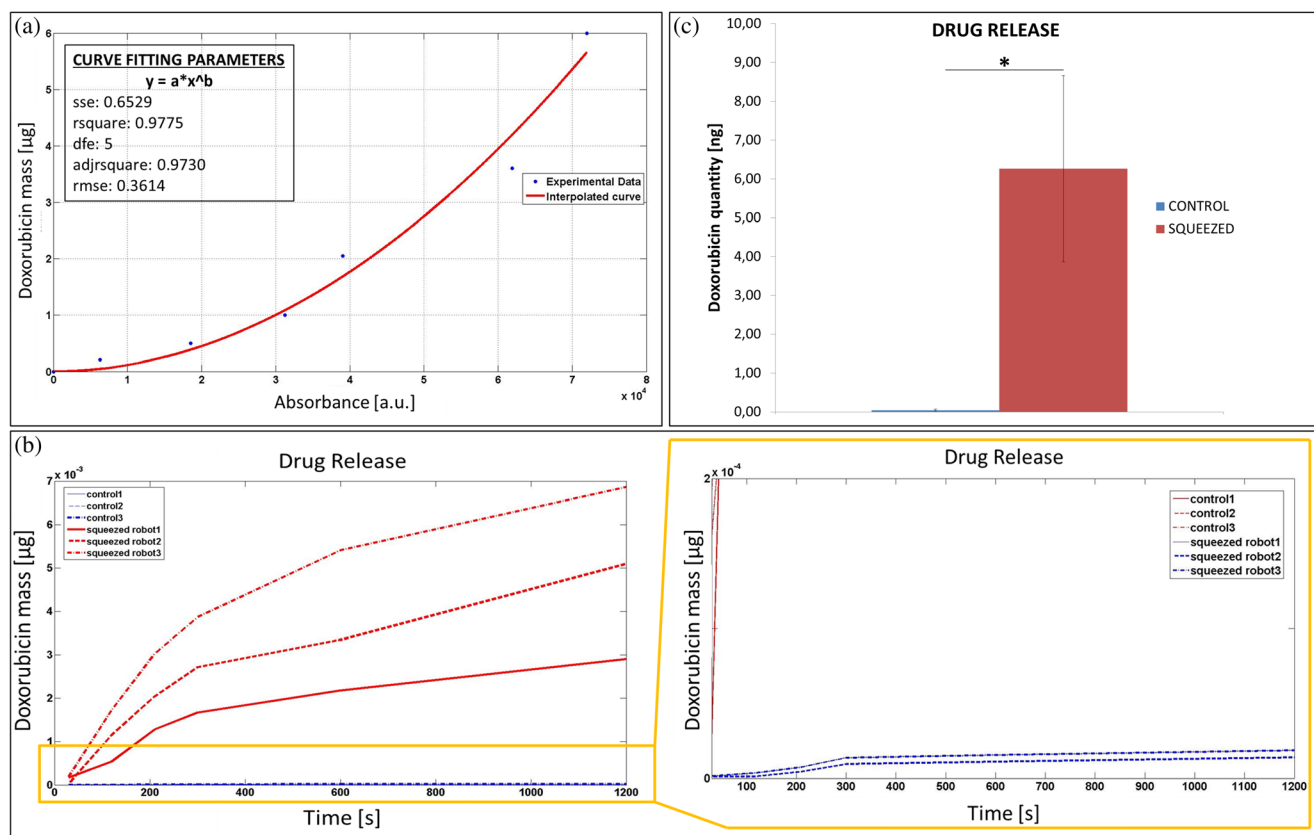


Fig. 7 **a** Doxorubicin calibration curve correlating the measured absorbance values with the doxorubicin amount dissolved in water. **b** Amount of drug released in 20 min by docked robots and controls and expanded view of the release curve, to better evaluate the amount of drug

released from the undocked robots; **c** Overall drug quantity released in 20 min from the two sample types (mean values \pm standard deviations). * $p < 0.05$

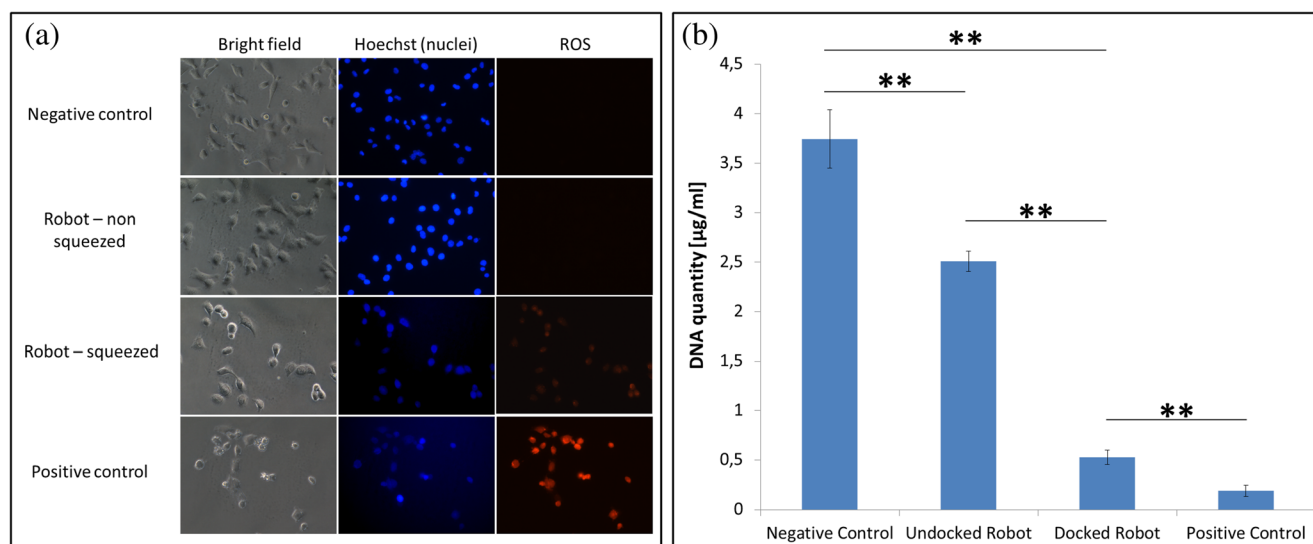


Fig. 8 Results of *in vitro* tests, performed on a human urinary bladder carcinoma cell line (T24). “Negative control” refers to non treated cells; “Undocked robot” refers to cells treated by immersing the carrier in the culture well, without squeezing it, for 20 min; “Docked robot” refers to cells treated by immersing the carrier, docked to the piston, in the culture well for 20 min; “Positive control” refers to cells treated with 10 μg/mL

doxorubicin, directly dispersed in the culture medium. **a** Bright field and fluorescence images for the different sample types, 24 h after the treatment (nuclei in blue, ROS production in red). **b** DNA content (related to cancer cell proliferation rate) for the different sample types, 72 h after the treatment. **=p<0.01

4 Conclusion

This paper presents a novel millirobot for targeted drug delivery. The system can be used for tumor treatment and, more generally, for the delivery of drugs and regenerative factors in body lumens such as the spine, the urinary system, the pancreas or the ovary.

The robot components were fabricated by using a biocompatible elastomer (polydimethylsiloxane) including small permanent magnets. NdFeB magnetic powders embedded in the carrier allowed to differentiate the properties of the two robot components, thus enabling their independent magnetic control. A doxorubicin-loaded hydrogel based on 0.25 % agar and 1 % gelatin was embedded in the carrier. Finite element model simulations predicted an overall hydrogel deformation of 38 %, due to the magnetic attraction between the carrier and the piston.

It has been demonstrated that robot locomotion and docking procedure can be performed wirelessly using magnetic fields. The proposed release mechanism, based on the mechanical compression of a drug-loaded matrix, was reliable and allowed to release ~6 ng of doxorubicin in 20 min. The drug amount released by non-squeezed robots, in the same time interval, was two orders of magnitude smaller. *In vitro* tests on human bladder cancer cells confirmed that the doxorubicin released by the squeezed robots was sufficient to trigger the desired therapeutic (anti-cancer) effects.

The proposed system may enable highly reliable targeted therapy in locations that are currently reachable only by means of systemic drug administration or through low-dexterity instruments.

Acknowledgments The authors would like to thank Mr. Tommaso Mazzocchi for his support with Abaqus simulations, Mr. Nicodemo Funaro and the staff of The BioRobotics Institute mechanical workshop for 3D printing. This work was supported in part by the GeT Small project (TarGeted Therapy at Small Scale), funded by the Scuola Superiore di Studi Universitari e di Perfezionamento Sant’Anna (Pisa, Italy). Pierre Dupont acknowledges support by the US National Science Foundation under grant IIS-1208509 and by the Wyss Institute for Biologically Inspired Engineering.

References

- J.J. Abbott, Z. Nagy, F. Beyeler, B.J. Nelson, Robotics in the small. *IEEE Robot. Autom. Mag.* **14**, 3 (2007)
- J.J. Abbott, K.E. Peyer, M. Cosentino Lagomarsino, L. Zhang, L. Dong, I.K. Kaliakatsos, B.J. Nelson, How should microrobots swim? *Int. J. Robot. Res.* **28**, 11–12 (2009)
- M. Alvarado-Velez, S.B. Pai, R.V. Bellamkonda, Hydrogels as carriers for stem cell transplantation. *IEEE Trans. Biomed. Eng.* **61**, 5 (2014)
- D. Armani, Deniz, C. Liu, N. Aluru, Re-configurable fluid circuits by PDMS elastomer micromachining. *Proc. IEEE Micr. Elect.* (1999)
- M. Arruebo, Drug delivery from structured porous inorganic materials. *Wiley Interdiscip. Rev. Nanomed. Nanobiotechnol.* **4**, 1 (2012)
- M. Arruebo, R. Fernández-Pacheco, M.R. Ibarra, J. Santamaría, Magnetic nanoparticles for drug delivery. *Nano Today* **2**, 3 (2007)
- C. Bergeles, G. Yang, From passive tool holders to microsurgeons: safer, smaller, smarter surgical robots. *IEEE Trans. Biomed. Eng.* **61**, 5 (2013)
- R. Cassano, S. Trombino, in *Advanced Polymers Medicine*, ed. by F. Puoci (Springer, Switzerland, 2015), pp. 341–370
- U.H. Chee, E.R. LeMoure, Catheter with atraumatic drug delivery tip, U.S. Patent No. 5,380,307. 10 Jan. 1995
- R. Chenga, F. Menga, C. Denga, H. Kloka, Z. Zhong, Dual and multi-stimuli responsive polymeric nanoparticles for programmed site-specific drug delivery. *Biomaterials* **34**, 14 (2013)

- D. de Lanauze, O. Felfoul, J. Turcot, M. Mohammadi, S. Martel, Three-dimensional remote aggregation and steering of magnetotactic bacteria microrobots for drug delivery applications, *Int. J. Robot. Res.* **32**, 1 (2013)
- E. Diller, S. Floyd, C. Pawashe, M. Sitti, Control of multiple heterogeneous magnetic microrobots in two dimensions on nonspecialized surfaces. *IEEE Trans. Robot.* **28**, 1 (2012)
- E. Diller, J. Giltinan, M. Sitti, Independent control of multiple magnetic microrobots in three dimensions. *Int. J. Robot. Res.* **32**, 5 (2013)
- A. Eqtami, O. Felfoul, P. E. Dupont, MRI-powered closed-loop control for multiple magnetic capsules, in *Proc. IEEE Int. Conf. Int. Syst.* (2014)
- T.W.R. Fountain, P.V. Kailat, J.J. Abbott, Wireless control of magnetic helical microrobots using a rotating-permanent-magnet manipulator, in *Proc. IEEE Int. Conf. Robot. Autom.* (2010)
- S. Fusco, F. Ullrich, J. Pokki, G. Chatzipirpiridis, B. Özkal, K.M. Sivaraman, O. Ergeneman, S. Pané, B.J. Nelson, Microrobots: a new era in ocular drug delivery. *Expert Opin. Drug Deliv.* **11**, 11 (2014)
- S. Gnani, L. di Blasio, C. Tonda-Turo, A. Mancardi, L. Primo, G. Ciardelli, G. Gambarotta, S. Geuna, I. Perroteau, Gelatin-based hydrogel for vascular endothelial growth factor release in peripheral nerve tissue engineering, *J. Tissue Eng. Regen. Med.* (2014)
- T. Hoare, B.P. Timko, J. Santamaria, G.F. Goya, S. Irusta, S. Lau, D.S. Kohane, Magnetically triggered nanocomposite membranes: a versatile platform for triggered drug release. *Nano Lett.* **11**, 3 (2011)
- S. Jeong, H. Choi, J. Choi, C. Yu, J.-o. Park, S. Park, Novel electromagnetic actuation (EMA) method for 3-dimensional locomotion of intravascular microrobot. *Sensors Actuators A Phys.* **157**, 1 (2010)
- G. Kósa, P. Jakab, G. Székely, N. Hata, MRI driven magnetic microswimmers. *Biomed. Microdevices* **14**, 1 (2011)
- M.P. Kummer, J.J. Abbott, B.E. Kratochvil, R. Borer, A. Sengul, B.J. Nelson, OctoMag: an electromagnetic system for 5-DOF wireless micromanipulation. *IEEE Trans. Robot.* **26**, 6 (2010)
- J. Lammer, K. Malagari, T. Vogl, F. Pilleul, A. Denys, A. Watkinson, M. Pitton, G. Sergent, T. Pfammatter, S. Terraz, Y. Benhamou, Y. Avajon, T. Gruenberger, M. Pomoni, H. Langenberger, M. Schuchmann, J. Dumortier, C. Mueller, P. Chevallier, R. Lencioni, Prospective randomized study of doxorubicin-eluting-bead embolization in the treatment of hepatocellular carcinoma: results of the PRECISION V study. *Cardiovasc. Intervent. Radiol.* **33**, 1 (2010)
- Y. Li, R.S. Shawgo, B. Tyler, P.T. Henderson, J.S. Vogel, A. Rosenberg, P.B. Storm, R. Langer, H. Brem, M.J. Cima, In vivo release from a drug delivery MEMS device. *J. Control. Release* **100**, 2 (2004)
- A.W. Mahoney, J.C. Sarrazin, E. Bamberg, J.J. Abbott, Velocity control with gravity compensation for magnetic helical microswimmers. *Adv. Robot.* **25**, 8 (2011)
- R. Mhanna, F. Qiu, L. Zhang, Y. Ding, K. Sugihara, M.y Zenobi-Wong, B.J. Nelson, Artificial Bacterial Flagella for Remote-Controlled Targeted Single-Cell Drug Delivery, *Small*, 1010 (2014)
- B.J. Nelson, I.K. Kaliakatsos, J.J. Abbott, Microrobots for minimally invasive medicine, *Annu. Rev. Biomed. Eng.* **12**, (2010)
- S. Palagi, B. Mazzolai, C. Innocenti, C. Sangregorio, L. Beccai, How does buoyancy of hydrogel microrobots affect their magnetic propulsion in liquids? *Appl. Phys. Lett.* **102**, 12 (2013)
- V. Panagiotis, M.R. Akhavan-Sharif, P. E. Dupont, Motion planning for multiple millimeter-scale magnetic capsules in a fluid environment, in *Proc. IEEE Int. Conf. Robot. Autom.* (2012)
- T. Qiu, T. Lee, A. G. Mark, K.I. Morozov, R. Münster, O. Mierka, S. Turek, A. M. Leshansky, P. Fischer, Swimming by reciprocal motion at low Reynolds number, *Nat. Commun.* **5** (2014)
- L. Ricotti, A. Menciassi, Engineering stem cells for future medicine. *IEEE Trans. Biomed. Eng.* **60**, 3 (2013)
- L. Ricotti, A. Cafarelli, V. Iacovacci, L. Vannozzi, A. Menciassi, Advanced micro-nano-bio systems for future targeted therapies. *Curr. Nanosci.* (2015). doi:10.2174/1573413710666141114221246
- M.S. Sakar, A. Meo, J. Moller, B.E. Kratochvil, C.S. Chen, V. Vogel, B.J. Nelson, Three-dimensional, automated magnetic biomanipulation with subcellular resolution, in *Proc. IEEE Int. Conf. Robot. Autom.* (2013)
- D. Seliktar, Designing cell-compatible hydrogels for biomedical applications. *Science* **336**, 6085 (2012)
- L.J. Sliker, G. Ciuti, Flexible and capsule endoscopy for screening, diagnosis and treatment. *Expert Rev. Med. Devices* **11**, 6 (2014)
- L. Smith, M.B. Watson, S.L. O'Kane, P.J. Drew, M.J. Lind, L. Cawkwell, The analysis of doxorubicin resistance in human breast cancer cells using antibody microarrays. *Mol. Cancer Ther.* **5**, 8 (2006)
- K. Storz, Hysteroscopes from KARL STORZ (2015), https://www.karlstorz.com/cps/rde/xcr/karlstorz_assets/ASSETS/3079310.pdf
- S.N. Tabatabaei, J. Lapointe, S. Martel, Shrinkable hydrogel-based magnetic microrobots for interventions in the vascular network. *Adv. Robot.* **25**, 8 (2012)
- S. Tamaz, R. Gourdeau, A. Chanu, J. Mathieu, S. Martel, Real-time MRI-based control of a ferromagnetic core for endovascular navigation. *IEEE Trans. Biomed. Eng.* **55**, 7 (2008)
- J. Tao, Q. Lu, D. Wu, P. Li, B. Xu, W. Qing, M. Wang, Z. Zhang, W. Zhang, microRNA-21 modulates cell proliferation and sensitivity to doxorubicin in bladder cancer cells. *Oncol. Rep.* **25**, 6 (2011)
- B.P. Timko, T. Dvir, D.S. Kohane, Remotely triggerable drug delivery systems. *Adv. Mater.* **22**, 44 (2010)
- J.D. Tobias, L. Oakes, N.K. Foreman, H. Mahmoud, Percutaneous lumbar intrathecal catheter for the administration of chemotherapy. *Med. Pediatr Oncol* **19**, 4 (1991)
- C. Tonda-Turo, S. Gnani, F. Ruini, G. Gambarotta, E. Goffredi, V. Chiono, I. Perroteau, G. Ciardelli, Development and characterization of novel agar and gelatin injectable hydrogel as filler for peripheral nerve guidance channels, *J. Tissue Eng. Regen. Med.* (2014)
- S.P. Woods, T.G. Constandinou, Wireless capsule endoscope for targeted drug delivery: mechanics and design considerations. *IEEE Trans. Biomed. Eng.* **60**, 4 (2012)
- S. Yim, M. Sitti, Shape-programmable soft capsule robots for semi-implantable drug delivery. *IEEE Trans. Robot.* **28**, 5 (2012)
- K.W. Yung, P.B. Landecker, D.D. Villani, An analytic solution for the force between two magnetic dipoles. *Magn. Electr. Sep.* **9**, 1 (1998)
- M. Zaaroor, G. Kosa, A. Peri-Eran, I. Maharil, M. Shoham, D. Coldsher, Morphological study of the spinal canal content for subarachnoid endoscopy. *Minim. Invasive Neurosurg.* **49**, 4 (2006)
- X. Zhao, J. Kimb, C.A. Cezar, N. Huebsch, K. Lee, K. Bouhadir, D.J. Mooney, Active scaffolds for on-demand drug and cell delivery. *Proc. Natl. Acad. Sci. U. S. A.* **108**, 1 (2011)